# Extremely well isolated two-dimensional spin-$\frac{1}{2}$ antiferromagnetic Heisenberg layers with a small exchange coupling in the molecular-based magnet CuPOF

D. Opherden,[1,2,*] N. Nizar,[3] K. Richardson,[3] J. C. Monroe,[4] M. M. Turnbull,[4] M. Polson,[5] S. Vela,[6] W. J. A. Blackmore,[7] P. A. Goddard,[7] J. Singleton,[8] E. S. Choi,[9] F. Xiao,[10] R. C. Williams,[10] T. Lancaster,[10] F. L. Pratt,[11] S. J. Blundell,[12] Y. Skourski,[1] M. Uhlarz,[1] A. N. Ponomaryov,[1] S. A. Zvyagin,[1] J. Wosnitza,[1,2] M. Baenitz,[13] I. Heinmaa,[14] R. Stern,[14] H. Kühne,[1,†] and C. P. Landee[3,‡]

[1]*Hochfeld-Magnetlabor Dresden (HLD-EMFL) and Würzburg-Dresden Cluster of Excellence ct.qmat, Helmholtz-Zentrum Dresden-Rossendorf, 01328 Dresden, Germany*

[2]*Institut für Festkörper- und Materialphysik, TU Dresden, 01062 Dresden, Germany*

[3]*Department of Physics, Clark University, Worcester, Massachusetts 01610, USA*

[4]*Carlson School of Chemistry, Clark University, Worcester, Massachusetts 01610, USA*

[5]*Department of Chemistry, University of Canterbury, Private Bag 4800, Christchurch, New Zealand*

[6]*Laboratoire de Chimie Quantique, UMR 7177, CNRS-Universitéde Strasbourg, 4, rue Blaise Pascal, F-67000 Strasbourg, France*

[7]*Department of Physics, University of Warwick, Gibbet Hill Road, Coventry CV4 7AL, United Kingdom*

[8]*National High Magnetic Field Laboratory, Los Alamos National Laboratory, Los Alamos, New Mexico 87545, USA*

[9]*National High Magnetic Field Laboratory, Florida State University, Tallahassee, Florida 32310, USA*

[10]*Durham University, Centre for Materials Physics, South Road, Durham DH1 3LE, United Kingdom*

[11]*ISIS Facility, Rutherford Appleton Laboratory, Chilton, Didcot, Oxford OX11 OQX, United Kingdom*

[12]*Clarendon Laboratory, Department of Physics, University of Oxford, Park Road, Oxford OX1 3PU, United Kingdom*

[13]*Max Planck Institute for Chemical Physics of Solids, 01187 Dresden, Germany*

[14]*National Institute of Chemical Physics and Biophysics, Akadeemia tee 23, 12618 Tallinn, Estonia*

(Received 15 May 2020; revised 24 July 2020; accepted 27 July 2020; published 28 August 2020)

We report on a comprehensive characterization of the newly synthesized $Cu^{2+}$-based molecular magnet $[Cu(pz)_2(2\text{-}HOpy)_2](PF_6)_2$ (CuPOF), where pz = $C_4H_4N_2$ and 2-HOpy = $C_5H_4NHO$. From a comparison of theoretical modeling to results of bulk magnetometry, specific heat, $\mu^+$SR, ESR, and NMR spectroscopy, this material is determined as an excellent realization of the two dimensional square-lattice $S = \frac{1}{2}$ antiferromagnetic Heisenberg model with a moderate intraplane nearest-neighbor exchange coupling of $J/k_B = 6.80(5)$ K, and an extremely small interlayer interaction of about 1 mK. At zero field, the bulk magnetometry reveals a temperature-driven crossover of spin correlations from isotropic to $XY$ type, caused by the presence of a weak intrinsic easy-plane anisotropy. A transition to long-range order, driven by the low-temperature $XY$ anisotropy under the influence of the interlayer coupling, occurs at $T_N = 1.38(2)$ K, as revealed by $\mu^+$SR. In applied magnetic fields, our $^1$H-NMR data reveal a strong increase of the magnetic anisotropy, manifested by a pronounced enhancement of the transition temperature to commensurate long-range order at $T_N = 2.8$ K and 7 T.

DOI: 10.1103/PhysRevB.102.064431

## I. INTRODUCTION

The study of critical phenomena, related to phase transitions between exotic ground states that emerge from complex underlying electronic correlations, is a subject of high importance in the research of low-dimensional magnetism. As has been established by extensive theoretical work, in contrast to the cases of one- and three-dimensional magnetic lattices, the critical behavior and ground-state properties of two-dimensional (2D) lattice systems are strongly dependent on the symmetry of the interactions between the magnetic moments, e.g., Ising, $XY$, and Heisenberg types [1]. For instance, in accordance with Onsager's exact solution [2], the 2D spin-$\frac{1}{2}$ Ising antiferromagnet undergoes a Néel-type transition to long-range order at $T_N = 1.06J/k_B$ [3], where $J$ is the exchange strength between neighboring magnetic moments. In contrast, thermal fluctuations in the 2D quantum Heisenberg antiferromagnet (2D QHAF) prevent long-range order at any finite temperature, as was rigorously proven by Mermin and Wagner [4]. The 2D planar, or $XY$, magnetic lattice does not exhibit Néel-type order, despite the divergence of the susceptibility at finite temperatures. Instead, an unusual topological order with characteristic algebraic decay of the spin correlations was proposed by Berezinskii [5] and

*d.dmytriieva@hzdr.de
†h.kuehne@hzdr.de
‡CLandee@clarku.edu

Kosterlitz and Thouless [6]. Here, the formation of bound pairs of topological excitations, called vortex and antivortex states, characterizes the ordered state, where the unbinding of the vortex-antivortex pairs constitutes the Berezinskii-Kosterlitz-Thouless (BKT) transition, which occurs at $T_{\mathrm{BKT}} = 0.353J/k_{\mathrm{B}}$ for the $S = \frac{1}{2}$ case [7].

Advancing the experimental research of phase transitions and critical phenomena relies on the availability of well-defined model systems. In particular, a targeted synthesis and characterization of materials with interaction parameters that closely approximate those of theoretical model systems and yield energy scales of temperature and magnetic field that are accessible by existing experimental infrastructures is required. The effective Hamiltonian to describe a quasi-2D QHAF in an applied magnetic field is

$$\mathcal{H} = J\sum_{i,j}\left[S_i^x S_j^x + S_i^y S_j^y + (1-\Delta)S_i^z S_j^z\right] + J'\sum_{i,i'}\mathbf{S}_i\mathbf{S}_{i'} - g\mu_B\mu_0 H\sum_i \mathbf{S}_i, \quad (1)$$

where $J$ and $J'$ are the intra- and interlayer exchange couplings, and $\Delta$ scales the deviation from an ideal Heisenberg interaction to an easy-axis or easy-plane characteristic. The first sum in Eq. (1) is taken over nearest-neighbor (NN) spins in the quasi-2D planes, the second summation is over NN spins in adjacent layers, and the Zeeman term applies to all moments. For external magnetic fields smaller than the anisotropy field $H_{\mathrm{A}}$ and $T \ll J/k_{\mathrm{B}}$, the formation of anisotropic magnetic correlations is driven by the intrinsic anisotropy $\Delta$. Conversely, for fields exceeding $H_{\mathrm{A}} = \Delta \times H_{\mathrm{sat}}$, where $H_{\mathrm{sat}}$ denotes the saturation field, the anisotropy of magnetic correlations is mainly determined by the strength and direction of the applied magnetic field. In the Hamiltonian (1), a positive $J$ corresponds to an antiferromagnetic exchange, and $0 < \Delta \leqslant 1$ describes the degree of easy-plane, or $XY$, anisotropy.

The discovery of the high-temperature cuprate superconductors attracted great attention to the 2D spin-$\frac{1}{2}$ Heisenberg model [8–16]. Some of the undoped parent compounds, such as $Sr_2CuCl_2O_2$ and $La_2CuO_4$, are known to be excellent realizations of 2D spin-$\frac{1}{2}$ Heisenberg antiferromagnets with large nearest-neighbor exchange couplings of the order of 1000 K [17–20]. However, in contrast with the ideal 2D Heisenberg model, a transition to a Néel-type state at finite temperatures is observed for all materials reported up to now. This transition is often discussed in terms of finite interlayer interactions [21–24], spin anisotropy [3,25,26], dipolar anisotropy, and other symmetry-allowed contributions to the Hamiltonian [27].

Whereas the critical phenomena of several systems were mapped onto the BKT theory, such as the superfluid transition of thin $^4$He films [28], the solid-on-solid model [29], the two-dimensional melting [30], the superconducting transition of Josephson junctions [31], the collision physics of 2D atomic hydrogen [32], the loss of quasicoherence of a trapped degenerate quantum gas of rubidium atoms [33], and the magnetic van der Waals antiferromagnet in the atomically thin limit [34], a very clean bulk realization of the square 2D $XY$ Heisenberg lattice is lacking up to now. There are two main obstacles for the experimental realization of a 2D $XY$ antiferromagnet. One challenge relates to the unavoidable existence of finite interlayer interactions. In case of the 2D Heisenberg magnets, even an infinitesimal interlayer interaction is sufficient to perturb the critical behavior of the system and stabilize a conventional type of Néel order below a transition temperature $T_{\mathrm{N}}$ [35]. Second, a weak intrinsic easy-plane anisotropy constraints the temperature range of $XY$-type correlations. For the case of crystalline magnetic lattices of $Cu^{2+}$ ions, the exchange coupling between spin moments as well as the single-ion properties are almost isotropic.

Another approach to realize a well-defined investigation of the magnetic correlations in low-dimensional spin systems is by tuning the Zeeman terms of the effective Hamiltonian with the application of an external magnetic field. This gives rise to the unique possibility of probing a quasi-2D spin system with well-defined $XY$ anisotropy in the experiment. It was shown by quantum Monte Carlo calculations that the application of a magnetic field to an isotropic 2D Heisenberg antiferromagnet can be mapped onto the anisotropic 2D $XY$ model in zero field, where the strength of the spin-exchange anisotropy can be continuously tuned by the external field [36,37]. This overall context has triggered extensive and ongoing efforts to synthesize novel quasi-2D Heisenberg model materials with highly isolated layers and relatively small antiferromagnetic interaction energies, allowing for the investigation of field-induced effects in moderate applied magnetic fields. Molecular-based materials consisting of $3d$ transition-metal ions, such as copper, embedded into an organic matrix are of particular interest. The combination of different ligands gives the opportunity to engineer a wide range of materials with well-defined magnetic properties [38–48].

In this paper, we report a comprehensive investigation of the magnetic properties of the newly synthesized compound $[Cu(pz)_2(2\text{-}HOpy)_2](PF_6)_2$ (CuPOF), where pz = $C_4H_4N_2$ and 2-HOpy = $C_5H_4NHO$. The material is characterized by magnetometry, ESR, specific heat, $\mu^+$SR, and NMR. CuPOF is shown to be a very clean realization of the square 2D spin-$\frac{1}{2}$ Heisenberg lattice with moderate intralayer antiferromagnetic NN exchange, $J/k_{\mathrm{B}} = 6.80(5)$ K, and highly isolated magnetic layers, with $J'/J \simeq 10^{-4}$. A weak intrinsic easy-plane anisotropy, revealed by bulk magnetometry, yields a temperature-driven crossover of the spin-correlation anisotropy from isotropic Heisenberg to anisotropic $XY$-type behavior, which, under the influence of a finite interlayer coupling $J'$, constitutes a driving mechanism for a transition to long-range commensurate order. A strong increase of the transition temperature upon application of a magnetic field from 1.38(2) K at zero field to 2.8 K at 7 T is caused by the field-driven increase of the anisotropy of spin correlations.

## II. EXPERIMENTAL

The compound $[Cu(pz)_2(2\text{-}HOpy)_2](PF_6)_2$ was synthesized by using conventional solution chemistry techniques, described in detail in the Supplemental Material (SM) [49]. Slow evaporation of methanol solutions of the product, $[Cu(pz)_2(2\text{-}HOpy)_2](PF_6)_2$, (pz = pyrazine, 2-HOpy = 2-pyridone) produces thin, rectangular, green plates, typically 3 to 5 mm on a side and about 1 mm thick. The crystals extinguish well under polarized light and are dichroic.

X-ray data were obtained by using an Agilent Technologies Gemini Eos CCX-ray diffractometer using Cu-$K\alpha$ radiation ($\lambda = 1.5418$ Å) with $\omega$ scans using CrysAlisPro software [50] refined cell parameters and SCALE3 ABSPACK [51] scaling algorithm defined absorption corrections. Data were collected at 120 K. SHELXS97 [52] was used to solve the structures, which were refined via least-squares analysis using SHELXL-2016 [53]. All non-hydrogen atoms were refined anisotropically. Hydrogen atoms bonded to nitrogen atoms were located in the difference Fourier maps and their positions refined with fixed isotropic thermal parameters. The remaining hydrogen atoms were geometrically located and refined by using a riding model with fixed isotropic thermal parameters. The structure has been deposited with the Cambridge Crystallographic Data Centre (CCDC) (1553982). A Bruker D8 powder x-ray diffractometer was used to confirm the purity and phase of powdered samples prior to magnetic measurements.

Measurements of magnetic bulk properties between 1.8 and 310 K were carried out by using a Quantum Design MPMS-XL SQUID magnetometer with a 5 T magnet, as well as a vibrating sample magnetometer (VSM) Quantum Design PPMS with a 14 T magnet. Corrections were made to the data for the background signal of the sample holder, as well as diamagnetic contributions. Studies below 2 K were performed by employing a $^3$He cooling stage.

The high-field magnetization of CuPOF single crystals in pulsed fields up to 35 T and at temperatures of 0.37 and 1.4 K were performed at the Dresden High Magnetic Field Laboratory (HLD) at the Helmholtz-Zentrum Dresden-Rossendorf. Additional measurements of a polycrystalline sample in DC fields up to 35 T were done by using a vibrating sample magnetometer at the National High Magnetic Field Laboratory (NHMFL) in Tallahassee, as well as in pulsed fields up to 25 T at the NHMFL facility in Los Alamos. The results are fully consistent with the data from the HLD and can be found in the SM [49].

Room-temperature electron-spin resonance (ESR) studies were performed on polycrystalline material and single crystals of CuPOF, using a commercially available X-Band Bruker ESR spectrometer operating at 9.8 GHz at Clark University. EASYSPIN [54] was used to determine the $g$ factors and linewidths. Additional ESR measurements of angular-dependent spectra, as well as temperature-dependent spectra for field parallel to the $c$ axis, were performed at the HLD between 3 and 300 K at 9.4 GHz, employing an X-band Bruker ELEYSYS E500 ESR spectrometer. The obtained values of the anisotropic $g$ factor are consistent with the results measured at Clark University and are presented in the SM [49]. High-frequency ESR measurements along the crystallographic $c$ axis at 1.5 K and fields up to 16 T were performed at the HLD by using a home-built transmission-type tunable-frequency ESR spectrometer, similar to that described in Ref. [55], with a probe in Faraday configuration. These results can also be found in the SM [49].

Heat-capacity measurements between 1.8 and 300 K were performed by using a Quantum Design PPMS system. Furthermore, a $^3$He insert was used to record the heat capacity at temperatures down to 0.4 K. Powdered samples with masses of 1.065(5) and 1.832(5) mg, for measurements at $^4$He and $^3$He temperatures, respectively, were pressed into pellets and attached to the sample platforms by using Apiezon N grease. The addenda was determined from measurements with an empty sample holder and subtracted from the data to obtain the heat capacity of the sample.

Zero-field muon-spin relaxation ($\mu^+$SR) measurements on a polycrystalline sample were carried out by using the EMU spectrometer at the ISIS facility at the Rutherford Appleton Laboratory. The sample was mounted on a Ag backing plate and covered with a 12.5-$\mu$m-thick Ag foil mask before being inserted into a dilution refrigerator. Further technical details are provided in the SM [49].

$^1$H nuclear magnetic resonance (NMR) spectra were recorded using a commercial solid-state spectrometer. A standard Hahn spin-echo pulse sequence with stepped sweep of the carrier frequency was employed to record the broad-bandwidth spectra. The NMR probe was equipped with a single-axis goniometer for precise orientation of the magnetic field parallel to the crystallographic $c$ axis. The measurements at 1.6 K and above were performed in a 8 T high-resolution magnet equipped with a $^4$He flow cryostat.

## III. RESULTS

*a. Crystal structure.* $[Cu(pz)_2(2\text{-}HOpy)_2](PF_6)_2$ crystallizes in the orthorhombic space group *Cmca*. The asymmetric crystallographic unit comprises one $Cu^{2+}$ ion, two half-pyrazine molecules, one 2-pyridone molecule and two $PF_6^-$ ions. The local coordination sphere of the $Cu^{2+}$ ion is presented in Fig. S1 in the SM [49]. The $Cu^{2+}$ ion sits on a twofold axis (parallel to $b$), one coordinated, dissymmetric (N11/N14) pyrazine sits on the same twofold axis while the other pyrazine molecule (N21) lies across a mirror plane normal to the $a$ axis. The two $PF_6^-$ ions also lie on mirror planes such that there are five independent fluoride ions in each. The $Cu^{2+}$ coordination sphere exhibits a classic distorted Jahn-Teller octahedral geometry with four bridging pyrazine molecules in the equatorial plane [Cu–N = 2.05(1) Å] and elongated Cu–O bonds [2.285(1) Å] in the axial sites. The copper ion and all four bound nitrogens are coplanar as required by symmetry. The Cu–O1 bond is nearly perpendicular to the plane, making an angle of 1.0° with the normal to the plane. Crystal data and structure refinement parameters, as well as selected bond lengths and angles of CuPOF, are presented in Tables S1 and S2 in the SM [49].

The bridging pyrazine ligands link the $Cu^{2+}$ ions into a nearly square layer, see Fig. 1(a). The pyrazine rings exhibit a propeller twist relative to the Cu plane, with the N11 rings canted 66.9° and the N21 rings canted 53.1° out of the plane. This results in slightly different Cu–Cu distances of 6.676 Å through the N11 ring and 6.680 Å through the N21 ring. The layers are further separated by the $PF_6^-$ anions, which are located in the pockets between the 2-pyridone ligands, resulting in a minimum Cu–Cu distance in adjacent layers of 13.097 Å.

The structure of CuPOF possesses a hidden canting, see Fig. 1(b). The Cu-pyrazine layers lie in the *ab* plane (into the page and horizontal) while the Cu-oxygen bonds are nearly parallel to the $c$ axis but canted by ±1.0° towards $b$. Within each layer, the canting is in the same direction but adjacent layers are canted in the opposite direction. A similar canting

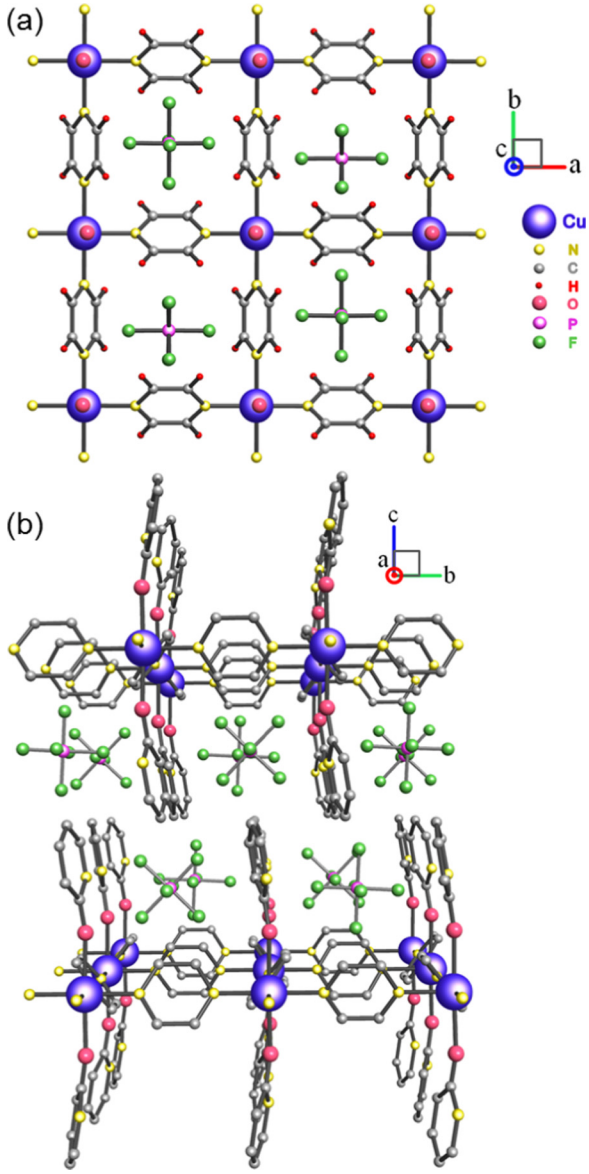


FIG. 1. (a) View of the Cu-pyrazine layers of CuPOF along the $c$ axis. The 2-pyridone molecules extend normal to the planes and are coordinated to the copper atoms through the oxygens. The uncoordinated $PF_6^-$ anions occupy vacancies in the lattice. (b) View of CuPOF along the $a$ axis. The Cu-pyrazine layers extend horizontally and into the page. The interdigitation of the 2-pyridone molecules leads to the extreme isolation of the layers. The 2-pyridone molecules within one layer are all canted in the $+b$ direction while the molecules in the adjacent layers cant in the $-b$ direction.

is seen in the orientation of the pyridone rings; they are alternately tilted by 8.7° away from the normal to the Cu-pyrazine planes. The chemical equivalence of the 2-pyridone molecules is confirmed by our $^{13}C$ magic-angle spinning (MAS) NMR spectroscopy (see Fig. S11 in the SM [49]).

*b. Magnetometry.* The magnetic susceptibility of a polycrystalline sample of CuPOF is shown in Fig. 2 and yields a rounded maximum near 6.8 K. At higher temperatures ($T >$ 40 K), the data are well described by a Curie-Weiss law with a Curie constant of 0.440(5) emuG$^{-1}$ mol$^{-1}$ K and a Curie-

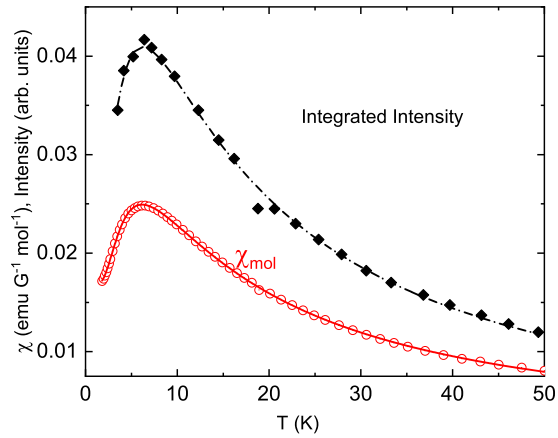


FIG. 2. Temperature dependence of the powder susceptibility (circles) in emuG$^{-1}$ mol$^{-1}$ and the integrated ESR intensity at 9.4 GHz (diamonds) in arbitrary units. The red line shows the best fit of the 2D QHAF model calculations to the magnetic susceptibility of a polycrystalline sample. The black dash-dotted line represents the fit of the same model to the integrated ESR intensity of a polycrystalline CuPOF sample.

Weiss temperature $\Theta_{CW} = -5.2(6)$ K, indicating a small antiferromagnetic interaction. Accordingly, the data were compared with the susceptibility of a 2D $S = \frac{1}{2}$ Heisenberg antiferromagnet [56] in which the Curie constant, exchange strength $J$, and small paramagnetic impurity fraction were adjusted. The best agreement between data and the model calculations, denoted by the red curve in Fig. 2, is obtained with $C = 0.445(5)$ emuG$^{-1}$ mol$^{-1}$ K, $J/k_B = 6.80(5)$ K, and 1.1(1)% paramagnetic contribution. The agreement between the Curie constants from the Curie-Weiss model and the 2D QHAF model is excellent, with their values corresponding to an average $g$ value of 2.17. The average $g$ factor has been determined at room temperature by using ESR and was found to be $\langle g \rangle = 2.15$.

The existence of two distinct pyrazine molecules in the unit cell allows for the possibility of a rectangular magnetic lattice in which the exchange strengths ($J$ and $\alpha J$, $0 \leqslant \alpha \leqslant 1$) along the $a$ and $b$ axes are different. This possibility has been tested by comparing the susceptibility data to the susceptibilities of a rectangular 2D QHAF [57,58] for various values of $J$ and $\alpha$. The square-lattice ($\alpha = 1$) case gives by far the best fit and it is possible to rule out any rectangular contribution with $\alpha < 0.96$.

The low-temperature static susceptibility of a single crystal of CuPOF at 0.1 T is shown in the inset of Fig. 3. The out-of-plane DC susceptibility ($H \parallel c$) has a minimum at 1.86(5) K, whereas, for a field applied in the $ab$ plane ($H \perp c$), the DC susceptibility steadily decreases to the lowest measured temperature. The minimum in the out-of-plane susceptibility at $T_{co}$ indicates the presence of $XY$ anisotropy, where, with decreasing temperature, the correlation of spin moments crosses from isotropic to easy-plane behavior. The temperature-dependent out-of-plane susceptibility at different magnetic fields is presented in the main panel of Fig. 3. With increasing magnetic field, the broad minimum of the static susceptibility shifts to higher temperatures, as indicated by the

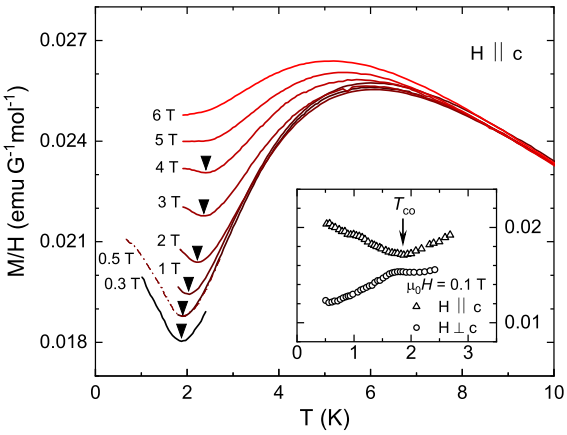


FIG. 3. Temperature dependence of the out-of-plane molar susceptibility of a single-crystalline sample of CuPOF at different magnetic fields. The solid black triangles in the main panel indicate the crossover temperature $T_{co}$, as discussed in the main text. The inset shows the low-temperature susceptibility of a single crystal of CuPOF. The data were collected in a field of 0.1 T. The susceptibilities normal to the plane and within the *ab* plane are represented by the open triangles and circles, respectively. The vertical arrow indicates the crossover temperature $T_{co}$ for $M/H \parallel c$ at 1.86(5) K. The broad anomaly of the in-plane static susceptibility at about 1.6(1) K is attributed to a background contribution.

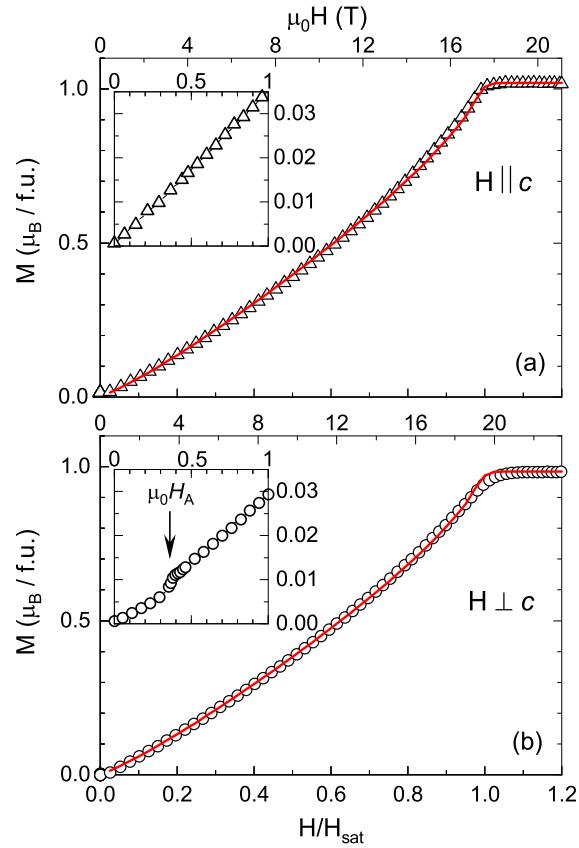


FIG. 4. Magnetization of single-crystalline CuPOF at 0.37 K in (a) out-of-plane and (b) in-plane direction and comparison with the respective QMC calculations (red line). The insets show the magnetization at 0.5 K in magnetic fields up to 1 T in an enlarged scale. The vertical arrow indicates the anisotropy field at $\mu_0 H_A = 0.36(1)$ T. The bottom axis represents the relative magnetic field $H/H_{sat}$. The corresponding absolute values of the magnetic fields are shown in the upper axis.

triangles. At fields above around 4 T, the minimum broadens and cannot be observed anymore.

The magnetization of a single crystal of CuPOF has been measured up to 1 T at 0.5 K, see the insets of Figs. 4(a) and 4(b). For a field parallel to the *c* axis, the magnetization monotonically increases over that range. In contrast, when the field is applied in the *ab* plane ($H \perp c$), a small spin-flop anomaly is observed at around 0.36(1) T.

The relative magnetization of single crystals of CuPOF was determined at several temperatures for fields up to 35 T both parallel to the *c* axis ($H \parallel c$) and within the layers ($H \perp c$). The experimental values at 0.37 K are presented in Figs. 4(a) and 4(b). The absolute values of the magnetization were obtained from a direct comparison with the magnetization recorded at 4 K for $H \parallel c$ (at 2 K for $H \perp c$) up to 14 T, by using a VSM magnetometer; see Fig. S3 in the SM [49]. For both magnetic-field orientations, the saturated moment is about 1 $\mu_B$ per formula unit, as expected for the $Cu^{2+}$ ion. The experimental data (symbols) are compared with quantum Monte Carlo (QMC) simulations (lines) for the 2D QHAF at the relative temperature $k_B T/J = 0.05$. Excellent agreement between the experimental data and the QMC simulations is found for both field orientations. Over the full field range, the deviation between experimental and theoretical data is below $\pm 1\%$ for $H \parallel c$ and below $\pm 2\%$ for $H \perp c$. The in- and out-of-plane saturation fields were determined as 17.6 and 19.6 T for $H \parallel c$ and $H \perp c$, respectively. In the mean-field approximation, the saturation field $H_{sat}$ is defined by the exchange strength *J*,

$$g\mu_B\mu_0 H_{sat} = 2zJS, \tag{2}$$

where $z = 4$ is the number of nearest-neighbor magnetic moments. The exchange strength can be computed from Eq. (2) by using the experimentally determined saturation fields and the respective *g* values $g_c = 2.29(1)$ at 1.5 K and $g_{ab} = 2.070(7)$ at room temperature; see the ESR section below. The obtained values, $J/k_B = 6.75(5)$ and 6.78(5) K, are in very good agreement with each other and with those determined from the susceptibility and specific-heat measurements.

*c. Electron-spin resonance.* The anisotropy of the room-temperature ESR spectrum of a single-crystalline CuPOF sample was investigated at 9.8 GHz. A single ESR line was observed for each field orientation; see Fig. S6 in the SM [49]. The resonance field, used to extract the electronic *g* factor and the spectral linewidth, was determined by modeling a nearly Lorentzian function to the experimentally obtained spectra [54,59,60]. The angular dependence of the *g* factor in the *ac*, *bc*, and *ab* planes indicates a strong planar-like anisotropy (Fig. S7 in the SM [49]), with $g_a = 2.073(2)$, $g_b = 2.066(4)$, and $g_c = 2.298(2)$.[1]

[1]The average values of the *g* factors from two independent ESR measurements on the single-crystalline CuPOF samples are presented here; for details see the SM [49].

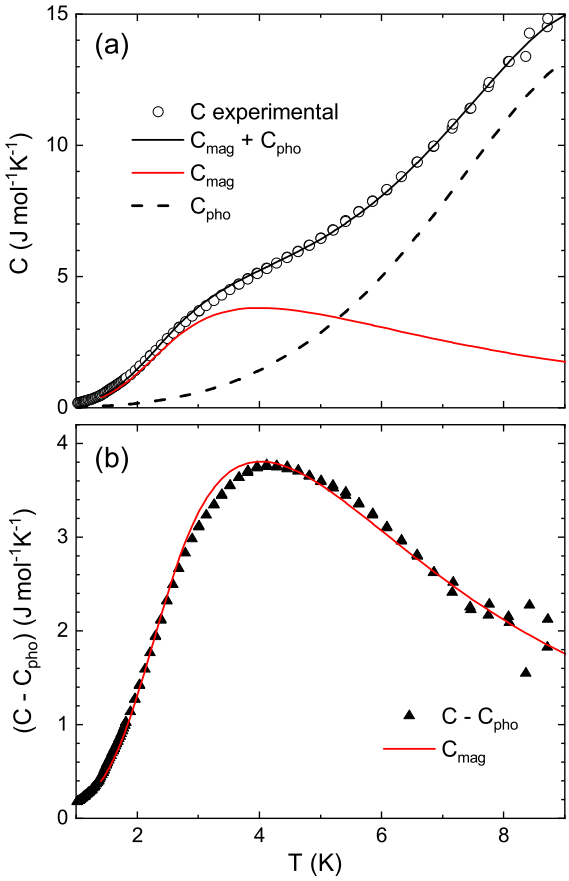


FIG. 5. (a) Temperature dependence of the normalized specific heat of CuPOF denoted as open black circles, with the black line representing the best fit to these data by a sum of magnetic (solid red line) and phonon (black dashed line) contributions, $C_{pho}$. (b) The black solid triangles represent $C_{mag}$, which is the difference between $C$ and $C_{pho}$.

The temperature-dependent integrated ESR-line intensity, scaling as the bulk susceptibility of the sample [61] is shown in Fig. 2 for temperatures between 3 and 50 K with the field applied along the $c$ axis. Analogously to the modeling of the DC susceptibility, the integrated ESR intensity was modeled, varying only the Curie constant, with fixed exchange coupling of $J/k_B = 6.80(5)$ K and a paramagnetic impurity percentage of 1.1(1)% (black dash-dotted line in Fig. 2).

High-frequency ESR spectroscopy at 1.5 K in the frequency range between 52 and 500 GHz revealed a single resonance mode with a linear frequency-field dependence (Fig. S9 in the SM [49]), yielding $g_c = 2.29(1)$.

*d. Specific heat.* The specific heat was measured between 0.4 and 300 K. The data increase smoothly from about 0.2 J mol$^{-1}$ K$^{-1}$ at 1 K, approaching 640 J mol$^{-1}$ K$^{-1}$ at 300 K. No sharp anomalies, corresponding to structural changes or ordering transitions, were observed in this range (Fig. S10 in the SM [49]). The data between 1 and 9 K are shown in Fig. 5(a) (black open circles) revealing a broad hump exceeding the normal phonon contribution. The data in this temperature range were analyzed as a sum of the magnetic specific heat of a 2D QHAF and a phononic contribution. The low-temperature lattice contribution to the specific heat, stemming from a complex phononic spectrum in the molecular-based material CuPOF, is best approximated by choosing a three-term polynomial with $C_{pho} = AT^3 + BT^5 + CT^7$. The magnetic specific heat was represented as a ratio of polynomials, similar to the approach used in a previous study [62], but is based on recent QMC simulations of the magnetic specific heat [63] that extended to lower relative temperatures. The range of validity for the square lattice is $0.15 \leqslant k_B T/J \leqslant 5.0$ (see SM and Table S4 therein [49]).

The resulting best fits to $C_{pho}$ and $C_{mag}$ are shown in Fig. 5(a). The sum of the two individual contributions appears as the solid black line and shows very good agreement with the experimental data. The modeling parameters are $J/k_B = 6.75(5)$ K, $A = 20.2\times10^{-3}$ J mol$^{-1}$ K$^{-4}$, $B = 16.6\times10^{-5}$ J mol$^{-1}$ K$^{-6}$, and $C = -23.7\times10^{-7}$ J mol$^{-1}$ K$^{-8}$. As seen in Fig. 5(a), the magnetic contribution dominates at lower temperatures. Including data at higher temperatures in the fitting process did not change the value of the exchange strength, since $C_{mag}$ is a rapidly decreasing fraction of the total specific heat. Figure 5(b) shows a direct comparison of the calculated magnetic specific heat (red line) to the difference between the total and estimated lattice specific heat (black triangles). The obtained exchange strength of $J/k_B = 6.75(5)$ K is in excellent agreement with that obtained from the susceptibility and magnetization results. Similar to the analysis of the bulk susceptibility, the specific-heat data were investigated in terms of the possibility of a rectangular magnetic lattice [63]. The results are consistent with a magnetic square lattice.

*e. Muon-spin relaxation.* Zero-field muon-spin relaxation ($\mu^+$SR) spectra [64] for CuPOF are shown in Fig. 6(a). Spontaneous oscillations in the asymmetry function $A(t)$, which is proportional to the spin polarization of the muon ensemble, see SM [49], were observed at low temperatures. An oscillating behavior of the muon-spin polarization is characteristic of the presence of quasistatic long-range magnetic order (LRO). The local magnetic field that results from LRO causes those muons with spin perpendicular to the local field to precess coherently at the frequency $\nu_i$, where $\nu_i$ is proportional to the magnitude of the local field $B_i$ at the $i$th muon site. Changes in the spectra are observed in measurements across the temperature range $0.1 < T < 2$ K, which is parametrized by modeling the asymmetry $A(t)$ with the relaxation function

$$A(t) = (A_0 - A_{bg})\cos(2\pi\nu t)e^{-\lambda_1 t} + A_{bg}e^{-\lambda_2 t}, \qquad (3)$$

where $A_0$ is the initial asymmetry at $t = 0$, the parameters $\nu$ and $\lambda_1$ are the precession frequency and relaxation rate of the oscillatory component, respectively. The parameters $A_{bg}$ and $\lambda_2$ account for the background muons and those with spin initially parallel to the local magnetic field.

The evolution of the parameters $A_0$, $\lambda_1$, and $\nu$ are shown in Figs. 6(b)–6(d). The precession frequency, see Fig. 6(d), which is proportional to the magnitude of internal magnetic field probed by the muon spins, shows a monotonic decrease from base temperature up to 1.4 K, but starts to rise again before becoming roughly constant above 1.5 K. A sharp maximum of $A_0$ and discontinuity of $\lambda_1$ are observed just below $T = 1.4$ K, coincident with the minimum of $\nu$.

The behavior of $\nu$, together with the peak of $A_0$ and the discontinuity of $\lambda_1$, suggest that CuPOF undergoes a magnetic phase transition around 1.4 K. However, unlike many

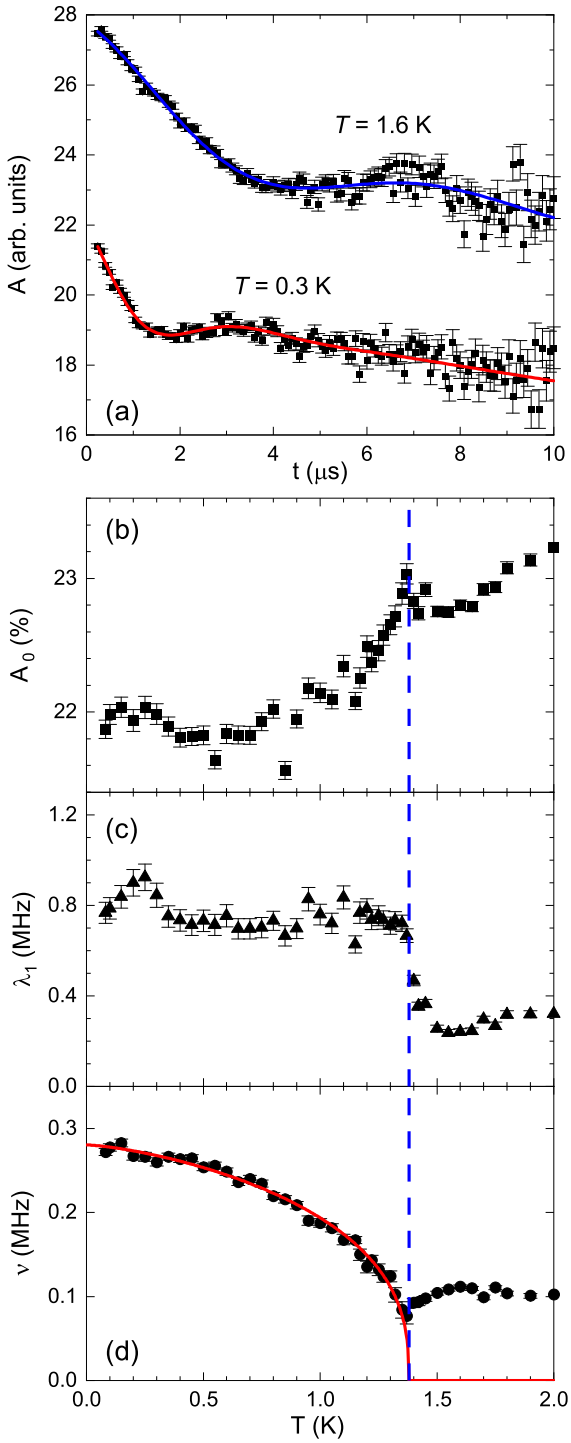


FIG. 6. (a) Representative $\mu^+$SR spectra of CuPOF at 0.30 and 1.60 K. Solid lines are fits to the data using Eq. (3). (b)–(d) Temperature dependence of the parameters $A_0$, $\lambda_1$, and $\nu$. The blue dashed line indicates $T_N = 1.38(2)$ K.

magnetic systems where the precession vanishes above $T_N$, the asymmetry still appears to show oscillatory behavior. Such an oscillatory signal is common in similar materials containing fluorine nuclei in the paramagnetic phase [65]. It arises because the electronic moments fluctuate outside of the muon time window and are consequently removed from the

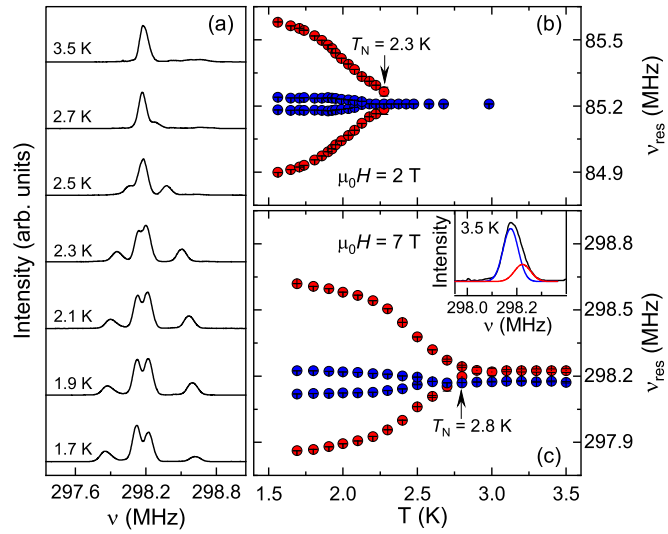


FIG. 7. (a) $^1$H-NMR spectra of CuPOF at selected temperatures in the regime of magnetic order, recorded at $\mu_0 H \parallel c = 7$ T. Temperature-dependent peak positions $\nu_{res}$ at out-of-plane fields of (b) 2 and (c) 7 T. Vertical arrows mark the onset temperature of LRO. The inset of panel (c) shows a typical $^1$H-NMR spectrum at 7 T and 3.5 K. Two nonequivalent hydrogen sites can be assigned in the paramagnetic regime.

spectrum, leaving the muon sensitive to the nuclear magnetic moments. In fluorinated materials, there are frequently muon sites where the positive muon sits close to the electronegative fluorine and enters a dipole-dipole coupled entangled state, leading to heavily damped, low-frequency oscillations [65]. A similar scenario for CuPOF is suggested, allowing identification of the antiferromagnetic transition temperature with the discontinuities in the modeled parameters.

To study the critical behavior close to the phase transition, we exclude the data above 1.4 K. To extract the critical exponent of the order parameter, the temperature dependence of the precession frequency was modeled by

$$\nu(T) = \nu(0)\left[1 - \left(\frac{T}{T_N}\right)^{\alpha}\right]^{\beta}. \tag{4}$$

The best fit with this model gives an ordering temperature $T_N = 1.38(2)$ K, a critical exponent $\beta = 0.37(2)$, and a phenomenological parameter $\alpha = 1.4(2)$. The resulting curve is shown in Fig. 6(d). Fixing $\alpha$ to unity and fitting the data between 0.85 and 1.40 K, i.e., closely below the transition temperature, results in very similar values for the critical exponent $\beta = 0.344(30)$ and the transition temperature $T_N = 1.382(10)$ K. Note that the critical temperature is consistent with the discontinuities found in Figs. 6(b) and 6(c).

*f. Nuclear magnetic resonance.* Selected $^1$H-NMR spectra, recorded for an out-of-plane field of 7 T and temperatures in the regime of long-range order, are presented in Fig. 7(a). Due to several nonequivalent hydrogen sites in the crystallographic unit cell, the resulting $^1$H-NMR spectrum is composed of many resonance peaks, and, therefore, rather complicated. Since the same qualitative temperature dependence was observed for all $^1$H lines of the spectrum, we consider in the following only selected lines with comparably little overlap.

TABLE I. Selected quasi-2D spin-$\frac{1}{2}$ Heisenberg square-lattice antiferromagnets with relevant exchange and anisotropy parameters. The exchange interaction $J$, ordering temperature $T_N$, $g$ factor, anisotropy field $H_A$, and saturation field $H_{sat}$ are experimentally determined. The inter- to intralayer coupling ratio $J'/J$ is estimated by the use of Eq. (5). The easy-plane anisotropy parameter $\Delta$ is calculated from the out-of-plane static susceptibility minimum by the use of Eq. (7). A direct estimate of $\Delta$ from ESR measurements in the ordered state [42] is denoted by $^{(\star)}$.

| Compound | Ref. | $J/k_B$ (K) | $T_N$ (K) | $k_BT_N/J$ | $J'/J$[a] | $\mu_0H_A$ (T) | $\mu_0H_{sat}$ (T) | $H_A/H_{sat}$ | $k_BT_{co}/J$ | $\Delta$[b] |
|---|---|---|---|---|---|---|---|---|---|---|
| $[Cu(pz)_2(2\text{-}HOpy)_2](PF_6)_2$ (CuPOF) | This work | 6.8 | 1.38 | 0.203 | $1.4\times10^{-4}$ | 0.36 | 17.6 $\parallel c$<br>19.5 $\perp c$ | $1.85\times10^{-2}$ | 0.274 | $0.9\times10^{-2}$ |
| (1) $Cu(pz)_2(ClO_4)_2$ | [40] | 17.5 | 4.25 | 0.243 | $8.8\times10^{-4}$ | 0.26 | 49 | $5.3\times10^{-3}$ | 0.257 | $4.6\times10^{-3}$ |
| (2) $Cu(pz)_2(BF_4)_2$ | [40] | 15.3 | 3.8 | 0.248 | $1.1\times10^{-3}$ | 0.25 | 43 | $5.8\times10^{-3}$ | 0.263 | $5.8\times10^{-3}$ |
| (3) $[Cu(pz)_2(NO_3)](PF_6)$ | [40] | 10.8 | 3.05 | 0.282 | $3.3\times10^{-3}$ | 0.007 | 30 | $2.3\times10^{-4}$ | 0.282 | $1.2\times10^{-2}$ |
| (4) $[Cu(pz)_2(HF_2)](PF_6)$ | [42] | 12.8 | 4.38 | 0.342 | $1.4\times10^{-2}$ | N.a. | 33.8 $\parallel c$<br>37.5 $\perp c$ | N.a. | N.a. | $3\times10^{-3\,(\star)}$ |
| (5) $[Cu(pz)_2(HF_2)](ClO_4)$ | [47] | 7.2 | 1.91 | 0.265 | $1.9\times10^{-3}$ | 0.08 | 20.2 | $4.0\times10^{-3}$ | N.a. | N.a. |
| (6) $[Cu(pz)_2(pyNO)_2](ClO_4)_2$ | [47] | 7.7 | 1.70 | 0.220 | $3.3\times10^{-4}$ | 0.11 | 21.9 | $5.0\times10^{-3}$ | N.a. | N.a. |
| (7) $[Cu(pz)_2(4\text{-}phpyNO)_2](ClO_4)$ | [47] | 7.5 | 1.63 | 0.217 | $2.8\times10^{-4}$ | 0.11 | 21.1 | $5.2\times10^{-3}$ | N.a. | N.a. |
| (8) $Sr_2CuO_2Cl_2$ | [71,72] | 1450 | 255 | 0.176 | $2.4\times10^{-5}$ | 0.7 | 4000[c] | $1.8\times10^{-4}$ | 0.221 | $8.3\times10^{-4}$ |

[a]Assuming $\Delta = 0$.
[b]Assuming $J' = 0$.
[c]Estimated value.

At temperatures above $T_N$ and an out-of-plane field of 2 T, a single, slightly nonsymmetric Gaussian-like line is observed. The larger field of 7 T allows one to assign two nonequivalent hydrogen sites with Gaussian lineshape in the paramagnetic regime, as exemplified by the blue and red fits to the spectrum at 3.5 K in the inset of Fig. 7(c).

As shown in Figs. 7(b) and 7(c), with decreasing temperature, the $^1$H-NMR line splits into two sets of doublets, revealing a phase transition to long-range order at 2.3 and 2.8 K for $\mu_0H \parallel c = 2$ and 7 T, respectively. The splitting of the NMR spectrum is a clear signature of commensurate antiferromagnetic order, where each of the two lines represents a sublattice magnetization of opposite local spin polarization. The observation of multiple doublets is caused by several nonequivalent hydrogen sites in the lattice, with coincidental overlap of the nuclear resonance frequency in the paramagnetic temperature regime. Due to the different hyperfine coupling constants of the corresponding $^1$H sites, this overlap is lifted in the ordered state. Considering the quasi-2D, almost-square structure of the $Cu^{2+}$ ions in CuPOF, the commensurate antiferromagnetic order is presumably of checkerboard type.

We note that the temperature dependence of the sublattice magnetization curves deviates from the mean-field-type behavior probed by the $\mu^+$SR precession frequency at zero field. The details of this field-induced behavior will be a subject of future, more detailed investigations by local-probe techniques.

As part of a thorough characterization of CuPOF, additional room-temperature $^{13}$C magic-angle spinning (MAS) NMR and $^{31}$P cryo-MAS NMR studies [66] were performed, and are presented in the SM (Figs. S11–S15) [49].

## IV. DISCUSSION

The ideal 2D QHAF is described by the Hamiltonian (1) for the case $J' = \Delta = 0$. Without applied field, the thermal fluctuations at arbitrarily low temperatures prevent a semiclassical order, regardless of the strength of the intralayer interaction $J$ [4]. Any small perturbations, such as a finite interlayer coupling or spin-exchange anisotropy, give rise to quasi-long-range order below a nonzero transition temperature. Hence, the ratio $k_BT_N/J$ can be treated as a measure of perturbations to the pure 2D QHAF [35]. It varies between zero for the 2D and 0.946(1) for the three-dimensional (3D) isotropic spin-$\frac{1}{2}$ Heisenberg model [67]. For typical molecular-based Cu-pyrazine materials, the reported values of $k_BT_N/J$ are between about 0.2 and 0.3, see Table I. The lowest ratio $k_BT_N/J = 0.176$ yet found applies to the inorganic material $Sr_2CuO_2Cl_2$, with a strong intralayer coupling of $J/k_B \simeq 1450$ K.

The nature of the transitions induced by finite $J'$ or $\Delta$ are fundamentally different. Whereas the interlayer coupling $J'$ induces a Néel state [35], a finite easy-plane or $XY$-like anisotropy yields a temperature-driven crossover of the spin correlations from isotropic Heisenberg to anisotropic $XY$-type behavior at a finite temperature $T_{co}$, predicted to lead to a topological BKT transition at $T_{BKT} < T_{co}$ [25,26,68].

In all bulk materials, finite interlayer couplings and magnetic anisotropies are present; see Table I for some selected cases. However, until now, there has been no theoretical framework that allows for an accurate experimental determination of $J'$ in the presence of a nonzero anisotropy $\Delta$ [40]. Still, the challenges associated with a clean experimental realization of the 2D QHAF can be discussed as follows: Predicted critical temperatures for the two limiting cases of a finite $J'$ with $\Delta = 0$, as well as that of a finite $\Delta$ with $J' = 0$ are presented in Fig. 8 as functions of the perturbation parameter, $J'/J$ or $\Delta$, respectively. The black curve represents the normalized Néel temperature, $k_BT_N/J$, of a 3D array of isotropic square 2D spin-$\frac{1}{2}$ Heisenberg planes with a coupling $J'$ between adjacent layers as a function of the exchange ratio

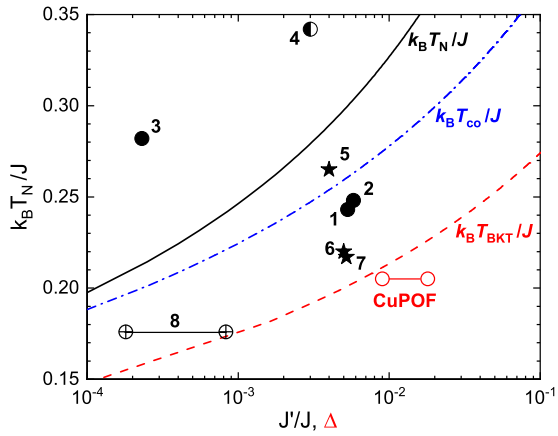


FIG. 8. Normalized Néel temperature as a function of $J'/J$ (black solid line), as well as the normalized crossover (blue dash-dotted line) and BKT transition temperatures (red dashed line) as functions of the anisotropy parameter $\Delta$. The normalized Néel temperature, $k_BT_N/J$, as a function of intrinsic easy-plane anisotropy, $\Delta$, for various Cu-pyrazine 2D QHAFs (○, ●, ◐, ★) and $Sr_2CuO_2Cl_2$ (⊕) [71,72]. The values indicated by ○ are for CuPOF, ● are from Ref. [40], ◐ is from Ref. [42], and ★ are from Ref. [47]. The numbers denote 2D QHAF compounds according to the labeling in Table I. The two distinct values for CuPOF and $Sr_2CuO_2Cl_2$ denote slightly different values of $\Delta$, determined from the DC susceptibility and low-field magnetization measurements, respectively.

$J'/J$ from Ref. [35]:

$$k_BT_N = \frac{4\pi\rho_s}{2.43 - \ln(J'/J)}, \tag{5}$$

where $\rho_s = 0.183J$ is the renormalized spin-stiffness constant. Note that the vertical axis is linear, whereas the horizontal axis is logarithmic and spans three orders of magnitude. The very weak decrease of the ordering temperature with reduction of the ratio $J'/J$ results from the exponential divergence of the correlation length of the 2D QHAF at low temperatures [17,69].

In the other limiting case with $J' = 0$ and finite $\Delta > 0$, quantum Monte Carlo calculations showed that, even for anisotropies as small as $10^{-3}$, the critical behavior of the magnetic lattice resembles that of the Berezinskii-Kosterlitz-Thouless universality class. A slow logarithmic decrease of the $T_{BKT}$ temperature with reduction of the spin-exchange anisotropy was determined as [68]

$$k_BT_{BKT} = \frac{2.22J}{\ln(330/\Delta)}, \tag{6}$$

as depicted by the red dashed line in Fig. 8.

From the comparison of these results, it is apparent that the interlayer interaction determines the ordering process for equal magnitudes of $J'/J$ and $\Delta$. Upon cooling from $T > J/k_B$, the onset of the 3D long-range order occurs before any signatures of the exchange anisotropy can be observed. The influence of the spin anisotropy is only relevant if the interlayer interaction $J'/J$ is significantly smaller than $\Delta$. Therefore, minimizing the interlayer spin interaction is of key importance for developing any material approximation to the ideal 2D QHAF.

In contrast to a strongly anisotropic spin system with $\Delta \simeq 1$, where the topological excitations of unpaired vortices and antivortices are formed well above $T_{BKT}$, a qualitatively different behavior is expected for a weakly anisotropic system with $\Delta \ll 1$ [26]. At high temperatures, the spin correlations can be well approximated as isotropic. With decreasing temperatures, the $XY$ anisotropy becomes relevant and stabilizes a planar spin configuration. The formation of vortices and antivortices starts in the regime of the temperature $T_{co}$, which indicates the crossover between isotropic and $XY$ behavior. Quantum Monte Carlo calculations revealed that the uniform susceptibility is very sensitive to this crossover phenomenon [26,68,70]. Whereas the in-plane susceptibility monotonically decreases with temperature below about $J/k_B$, a characteristic minimum of the out-of-plane susceptibility marks the crossover from isotropic to anisotropic behavior at $T_{co}$. The dependence of the crossover temperature on the spin anisotropy $\Delta$ can be described by the empirical expression [26]

$$k_BT_{co} = \frac{2.69J}{\ln(160/\Delta)}, \tag{7}$$

and is depicted by the dash-dotted blue line in Fig. 8.

Furthermore, in the presence of $XY$ spin anisotropy, the field-dependent magnetization is expected to yield a qualitatively different behavior for in- and out-of-plane orientations of the field at $T < T_{co}$. Below $T_{co}$, the antiferromagnetically coupled magnetic moments preferably fluctuate in the easy plane. The application of a magnetic field suppresses longitudinal spin fluctuations, effectively inducing an easy-plane anisotropy of spin correlations perpendicular to the field direction. For a field applied perpendicular to the intrinsic easy plane, this yields a monotonic increase of the magnetization. On the other hand, for a magnetic field applied in plane, when the Zeeman term becomes larger than the intrinsic anisotropy energy, the total spin polarization in the field direction is enhanced, yielding a slope increase of the magnetization curve at the anisotropy field $H_A$. Therefore, $H_A$ represents a measure of the spin-anisotropy parameter and can be estimated as $\Delta = H_A/H_{sat}$.

It is worth noting that, for most bulk realizations of the 2D QHAF model, the weak intrinsic $XY$ anisotropies do not stem from anisotropic exchange interactions. For the prevalent case of 2D QHAF materials based on $Cu^{2+}$ ions, the exchange between spins is almost isotropic. Typically, a weak anisotropy of a few percent of the isotropic superexchange interactions stems from crystal electric-field effects and related nonquenched orbital contributions. Commonly, the magnetic properties are then described by an effective-spin formalism, yielding an anisotropic $g$ factor. Equivalently, this anisotropy can be treated in terms of an anisotropic exchange of isotropic effective spin moments, as described by the Hamiltonian (1) [73].

Since the impact of a finite interlayer interaction $J'$ and spin anisotropy $\Delta$ on the critical behavior differ significantly [35,68], both parameters need to be experimentally determined for a newly synthesized compound to be accurately described as a quasi-2D QHAF. The strength of the antiferromagnetic exchange, $J$, as well as confirmation of lattice and exchange geometry being square rather than rectangular,

are of key importance. Secondary considerations include the possible existence of any next-nearest-neighbor interactions and spin-canting terms.

For the present case of CuPOF, from the comparison of theoretical modeling to our experimental results of DC susceptibility, specific heat, and high-field magnetization, a leading intralayer exchange constant $J/k_B = 6.80(5)$ K is consistently determined. All magnetic properties are in excellent agreement with theoretical predictions for the 2D square-lattice spin-$\frac{1}{2}$ Heisenberg antiferromagnet; see Figs. 2, 4, and 5. The resulting values of $J$, independently obtained by means of the aforementioned techniques, are in excellent agreement within experimental error. Additionally, the results of DC susceptibility and magnetic specific heat were analyzed in terms of a possible rectangular rather than a square magnetic in-plane structure [57,58] and are both fully consistent with the square-lattice case.

To further characterize CuPOF, the anisotropy of the electronic $g$ factor was investigated by means of ESR spectroscopy. A very weak in-plane anisotropy was found, with $g_a = 2.073(1)$ and $g_b = 2.066(3)$, in contrast with the out-of-plane $g$ factor $g_c = 2.298(2)$. Overall, the electronic $g$ factor anisotropy evinces a planar-like magnetic structure, with half filled $d_{x^2-y^2}$ orbitals oriented in the crystallographic $ab$ plane. The integrated ESR intensity, recorded for the out-of-plane field orientation at 9.4 GHz, is in excellent agreement with the bulk magnetic susceptibility, see Fig. 2, and confirms the intralayer antiferromagnetic coupling as $J/k_B = 6.80(5)$ K. Moreover, the linear frequency-field dependence of the ESR spectrum at 1.5 K, observed in the frequency range between 52 and 500 GHz, indicates the absence of a notable energy gap upon approaching the zero-field limit.

The absence of any specific-heat anomaly, see Fig. 5, which would be associated with the transition to long-range order at $T_N = 1.38(2)$ K, as determined by $\mu^+$SR, indicates a high isolation of the magnetic layers and related small change of the residual entropy at $T_N$ [74]. This sets the upper limit of the interlayer coupling as $J'/J < 10^{-2}$ [74]. Due to its pronounced low dimensionality, the thermodynamic properties of CuPOF show a very good agreement with those for an ideal isotropic 2D QHAF, where both the magnetic susceptibility and the specific heat exhibit a broad maximum at temperatures of the order of the nearest-neighbor exchange interaction $J/k_B$. On the other hand, the local-probe techniques $\mu^+$SR and NMR are highly sensitive to the onset of static internal-field components that are associated with long-range order. $\mu^+$SR was successfully used to determine the long-range-ordering temperature $T_N$ for a wide range of quasi-2D square-lattice quantum Heisenberg antiferromagnets [44,46,47,62].

In the case of CuPOF, the temperature evolution of the asymmetry parameter, precession frequency, and the relaxation rate of the oscillatory component of the $\mu^+$SR asymmetry relaxation function (3) revealed a zero-field transition to long-range order at $T_N = 1.38(2)$ K, see Fig. 6. Thus, the ratio $k_B T_N/J$ is found to be 0.203 for CuPOF, which is the smallest among all yet-characterized molecular-based materials with a magnetic lattice of $Cu^{2+}$ ions, compare Table I. By use of the empirical formula (5), the inter- to intralayer exchange ratio is obtained as $J'/J = 1.4\times10^{-4}$, with $J' \simeq 1$ mK. Since strictly isotropic exchange interactions, $\Delta = 0$, are assumed in the derivation of Eq. (5), $J'/J = 1.4\times10^{-4}$ sets an upper limit to the effective interlayer coupling. The dipolar interaction between nearest-neighbor $Cu^{2+}$ ions in adjacent layers, with a Cu–Cu distance of 13.097 Å, is estimated as about 1 mK. Therefore, the interlayer interaction likely stems from dipole-dipole coupling, rather than superexchange via the interlayer molecules. A planar magnetic structure with highly isolated layers is further supported by our density-functional theory (DFT) calculations [75,76]; see the SM [49]. Both the interlayer interactions and the next-nearest-neighbor intralayer interactions are negligible in comparison with the antiferromagnetic in-plane coupling mediated by the pyrazine molecules.

As discussed above, the anisotropy parameter $\Delta$ can be estimated from the low-temperature magnetization or low-field susceptibility measurements [26,40,47,68,72,77]. From the anisotropy field $\mu_0 H_A = 0.36(1)$ T, see inset of Fig. 4(b), the exchange anisotropy in CuPOF is evaluated as $\Delta = H_A/H_{sat} = 1.85(5)\times10^{-2}$. This results in the largest ratio $H_A/H_{sat}$ yet found for Cu-pyrazine-based layered materials; compare Table I. A slightly smaller anisotropy parameter is estimated from the out-of-plane DC susceptibility at 0.1 T; see inset of Fig. 3. Employing the empirical Eq. (7), derived for the case of $J' = 0$, the anisotropy parameter $\Delta = 0.9(2)\times10^{-2}$ is determined. The qualitative behavior of the field-dependent magnetization (Fig. 4) and temperature-dependent DC susceptibility (Fig. 3) are in very good agreement with calculations for a 2D QHAF with an $XY$ anisotropy of 1%–2% of the intralayer coupling [26,68], and resembles the characteristic behavior of previously studied Cu-pyrazine-based compounds [40,47,72].

To evaluate the relevant perturbations with respect to the ideal 2D QHAF and to shed light on the driving mechanism of the long-range order in CuPOF, the normalized Néel temperature $k_B T_N/J$ is shown as a function of the evaluated spin anisotropy $\Delta$ in Fig. 8 and compared with other molecular-based quasi-2D QHAFs. Where possible, the parameter $\Delta$ was determined from experimental values of $H_A/H_{sat}$ for the compounds labeled by black solid circles and stars. The two values for the inorganic compound $Sr_2CuO_2Cl_2$ are based on $H_A/H_{sat} = 1.8\times10^{-4}$ [19] and the minimum of the out-of-plane DC susceptibility $k_B T_{co}/J = 0.221$ [72], which corresponds to $\Delta = 8.3\times10^{-4}$, see Table I. The experimental values are compared with the theoretical expectation of the BKT transition temperature for a weakly anisotropic 2D QHAF, described by the empirical function (6).

For highly isolated quasi-2D materials, such as $Sr_2CuO_2Cl_2$ with $J'/J = 3\times10^{-5}$, the experimentally observed value of $k_B T_N/J$ is very close to the prediction of $k_B T_{BKT}/J$ (red dashed line in Fig. 8). Although the transitions to long-range and topological order at $T_N$ and $T_{BKT}$, respectively, are of a different nature, it was argued that, due to the exceptional low dimensionality of $Sr_2CuO_2Cl_2$, the long-range order is triggered by the inceptive BKT-type topological transition at $T_{BKT} \lesssim T_N$ [25,26]. Due to the finite interlayer coupling, a Néel-type antiferromagnetic order is stabilized at $T_N$, before the topological transition is completed. A very similar scenario is proposed for CuPOF, motivated by the close agreement between the experimentally obtained

value of $T_N$ and the theoretically predicted value of $T_{BKT}$. Moreover, the larger ratio $k_B T_N/J = 0.203$ as compared with $k_B T_N/J = 0.176$ for $Sr_2CuO_2Cl_2$, is attributed *only* to the stronger intrinsic spin anisotropy in CuPOF.

Furthermore, the field-driven increase of the crossover temperature $T_{co}$, observed by DC susceptibility, see Fig. 3, reveals the corresponding increase of the effective spin anisotropy. This field-induced spin anisotropy is evinced as well by the strong increase of the ordering temperature $T_N$ in applied magnetic field, as found by $^1$H-NMR spectroscopy, see Fig. 7. This strong increase of $T_N$ is attributed to the exceptional two-dimensionality of CuPOF, as compared with other less-isolated quasi-2D Cu-pyrazine-layered compounds, for which weaker field-induced changes of $T_N$ were reported [42,45,78,79]. The splitting of the $^1$H-NMR spectrum below the transition to long-range order is a clear signature of commensurate antiferromagnetic order.

In conclusion, we present a comprehensive characterization of the newly synthesized molecular-based compound $[Cu(pz)_2(2\text{-}HOpy)_2](PF_6)_2$ (CuPOF). Employing bulk magnetometry, specific heat, density-functional theory calculations, ESR, $\mu^+$SR, and NMR spectroscopy, CuPOF is characterized as an excellent realization of the 2D square-lattice spin-$\frac{1}{2}$ Heisenberg model with a moderate nearest-neighbor exchange interaction of $J/k_B = 6.80(5)$ K, and well-separated magnetic layers. The intralayer interaction is about four orders of magnitude larger than the estimated upper limit on the interlayer interaction, $J' \simeq 1$ mK. A weak intrinsic easy-plane anisotropy, revealed by bulk magnetometry, yields a temperature-driven crossover of the spin correlations from isotropic Heisenberg to anisotropic $XY$-type behavior and constitutes the driving mechanism of a transition to magnetic long-range order at $T_N = 1.38(2)$ K, as revealed by $\mu^+$SR spectroscopy. The application of a magnetic field normal to the easy plane yields a field-driven increase of the magnetic anisotropy, as shown by the evolution of the crossover temperature $T_{co}$ in the DC susceptibility data. The application of magnetic fields of several tesla leads to a strong increase of $T_N$, as revealed by $^1$H-NMR spectroscopy, in agreement with the pronounced two dimensionality of the magnetic lattice in CuPOF. As an outlook, our comprehensive characterization of $[Cu(pz)_2(2\text{-}HOpy)_2](PF_6)_2$ as a clean realization of a 2D square-lattice spin-$\frac{1}{2}$ Heisenberg antiferromagnet with moderate intralayer coupling and highly isolated magnetic layers calls for further studies of the field-induced effects on the anisotropy of the magnetic correlations [37], in particular by scattering and local-probe techniques.

Data presented in this paper resulting from the UK effort will be made available [80].

## ACKNOWLEDGMENTS

Christoph Klausnitzer from the Max Planck Institute for Chemical Physics of Solids is acknowledged for his strong technical support, and in memory of his lifetime achievements. We thank Paul Gape for experimental assistance with the muon experiment and for discussion of the data analysis. We acknowledge the support of HLD at HZDR, member of the European Magnetic Field Laboratory (EMFL). We acknowledge the support from the Deutsche Forschungsgemeinschaft (DFG) through SFB 1143 and the Würzburg-Dresden Cluster of Excellence on Complexity and Topology in Quantum Matter—ct.qmat (EXC 2147, project ID 390858490). Work at the National High Magnetic Field Laboratory is supported by NSF Cooperative Agreements No. DMR-1157490 and No. DMR-1644779, the State of Florida, the US DOE, and the DOE Basic Energy Science Field Work Project Science in 100 T. This project has received funding from the European Research Council (ERC) under the European Union's Horizon 2020 research and innovation program (Grant Agreement No. 681260). Part of this work was carried out at the STFC-ISIS facility and we are grateful for provision of beamtime. This work is supported by EPSRC (UK). S.A.Z. and A.N.P. acknowledge the support of DFG through ZV 6/2-2. I.H. and R.S. were supported by the European Regional Development Fund (Grant No TK134), and by the Estonian Research Council (PRG4, IUT23-7).

[1] L. J. de Jongh and A. R. Miedema, Adv. Phys. **23**, 1 (1974).
[2] L. Onsager, Phys. Rev. **65**, 117 (1944).
[3] H.-Q. Ding, J. Phys.: Condens. Matter **2**, 7979 (1990).
[4] N. D. Mermin and H. Wagner, Phys. Rev. Lett. **17**, 1133 (1966).
[5] V. L. Berezinskii, Sov. Phys. JETP **32**, 493 (1971).
[6] J. M. Kosterlitz and D. J. Thouless, J. Phys. C: Solid State Phys. **6**, 1181 (1973).
[7] H.-Q. Ding and M. S. Makivić, Phys. Rev. Lett. **64**, 1449 (1990).
[8] J. G. Bednorz and K. A. Müller, Z. Phys. B: Condens. Matter **64**, 189 (1986).
[9] P. W. Anderson, Science **235**, 1196 (1987).
[10] Z. Z. Sheng and A. M. Hermann, Nature (London) **332**, 55 (1988).
[11] A. Schilling, M. Cantoni, J. D. Guo, and H. R. Ott, Nature (London) **363**, 56 (1993).
[12] C. W. Chu, L. Gao, F. Chen, Z. J. Huang, R. L. Meng, and Y. Y. Xue, Nature (London) **365**, 323 (1993).
[13] S. N. Putilin, E. V. Antipov, O. Chmaissem, and M. Marezio, Nature (London) **362**, 226 (1993).
[14] A. J. Leggett, Nat. Phys. **2**, 134 (2006).
[15] J. R. Kirtley, C. C. Tsuei, Ariando, C. J. M. Verwijs, S. Harkema, and H. Hilgenkamp, Nat. Phys. **2**, 190 (2006).
[16] S. Graser, P. J. Hirschfeld, T. Kopp, R. Gutser, B. M. Andersen, and J. Mannhart, Nat. Phys. **6**, 609 (2010).
[17] S. Chakravarty, B. I. Halperin, and D. R. Nelson, Phys. Rev. Lett. **60**, 1057 (1988).
[18] B. Keimer, N. Belk, R. J. Birgeneau, A. Cassanho, C. Y. Chen, M. Greven, M. A. Kastner, A. Aharony, Y. Endoh, R. W. Erwin, and G. Shirane, Phys. Rev. B **46**, 14034 (1992).
[19] M. Greven, R. J. Birgeneau, Y. Endoh, M. A. Kastner, M. Matsuda, and G. Shirane, Z. Phys. B: Condens. Matter **96**, 465 (1995).
[20] M. Greven, R. J. Birgeneau, Y. Endoh, M. A. Kastner, B. Keimer, M. Matsuda, G. Shirane, and T. R. Thurston, Phys. Rev. Lett. **72**, 1096 (1994).

[21] B.-G. Liu, Phys. Rev. B **41**, 9563 (1990).
[22] N. Majlis, S. Selzer, and G. C. Strinati, Phys. Rev. B **45**, 7872 (1992).
[23] N. Majlis, S. Selzer, and G. C. Strinati, Phys. Rev. B **48**, 957 (1993).
[24] L. Siurakshina, D. Ihle, and R. Hayn, Phys. Rev. B **61**, 14601 (2000).
[25] H.-Q. Ding, Phys. Rev. Lett. **68**, 1927 (1992).
[26] A. Cuccoli, T. Roscilde, R. Vaia, and P. Verrucchi, Phys. Rev. Lett. **90**, 167205 (2003).
[27] T. Yildirim, A. B. Harris, O. Entin-Wohlman, and A. Aharony, Phys. Rev. Lett. **72**, 3710 (1994).
[28] D. J. Bishop and J. D. Reppy, Phys. Rev. Lett. **40**, 1727 (1978).
[29] H. J. F. Knops, Phys. Rev. Lett. **39**, 766 (1977).
[30] B. I. Halperin and D. R. Nelson, Phys. Rev. Lett. **41**, 121 (1978).
[31] D. J. Resnick, J. C. Garland, J. T. Boyd, S. Shoemaker, and R. S. Newrock, Phys. Rev. Lett. **47**, 1542 (1981).
[32] A. I. Safonov, S. A. Vasilyev, I. S. Yasnikov, I. I. Lukashevich, and S. Jaakkola, Phys. Rev. Lett. **81**, 4545 (1998).
[33] Z. Hadzibabic, P. Krüger, M. Cheneau, B. Battelier, and J. Dalibard, Nature (London) **441**, 1118 (2006).
[34] K. Kim, S. Y. Lim, J.-U. Lee, S. Lee, T. Y. Kim, K. Park, G. S. Jeon, C.-H. Park, J.-G. Park, and H. Cheong, Nat. Commun. **10**, 1 (2019).
[35] C. Yasuda, S. Todo, K. Hukushima, F. Alet, M. Keller, M. Troyer, and H. Takayama, Phys. Rev. Lett. **94**, 217201 (2005).
[36] D. P. Landau and K. Binder, Phys. Rev. B **24**, 1391 (1981).
[37] A. Cuccoli, T. Roscilde, R. Vaia, and P. Verrucchi, Phys. Rev. B **68**, 060402(R) (2003).
[38] F. M. Woodward, P. J. Gibson, G. B. Jameson, C. P. Landee, M. M. Turnbull, and R. D. Willett, Inorg. Chem. **46**, 4256 (2007).
[39] P. A. Goddard, J. Singleton, P. Sengupta, R. D. McDonald, T. Lancaster, S. J. Blundell, F. L. Pratt, S. Cox, N. Harrison, J. L. Manson, H. I. Southerland, and J. A. Schlueter, New J. Phys. **10**, 083025 (2008).
[40] F. Xiao, F. M. Woodward, C. P. Landee, M. M. Turnbull, C. Mielke, N. Harrison, T. Lancaster, S. J. Blundell, P. J. Baker, P. Babkevich, and F. L. Pratt, Phys. Rev. B **79**, 134412 (2009).
[41] J. L. Manson, K. H. Stone, H. I. Southerland, T. Lancaster, A. J. Steele, S. J. Blundell, F. L. Pratt, P. J. Baker, R. D. McDonald, P. Sengupta, J. Singleton, P. A. Goddard, C. Lee, M.-H. Whangbo, M. M. Warter, C. H. Mielke, and P. W. Stephens, J. Am. Chem. Soc. **131**, 4590 (2009).
[42] E. Čižmár, S. A. Zvyagin, R. Beyer, M. Uhlarz, M. Ozerov, Y. Skourski, J. L. Manson, J. A. Schlueter, and J. Wosnitza, Phys. Rev. B **81**, 064422 (2010).
[43] N. S. Headings, S. M. Hayden, R. Coldea, and T. G. Perring, Phys. Rev. Lett. **105**, 247001 (2010).
[44] A. J. Steele, T. Lancaster, S. J. Blundell, P. J. Baker, F. L. Pratt, C. Baines, M. M. Conner, H. I. Southerland, J. L. Manson, and J. A. Schlueter, Phys. Rev. B **84**, 064412 (2011).
[45] Y. Kohama, M. Jaime, O. E. Ayala-Valenzuela, R. D. McDonald, E. D. Mun, J. F. Corbey, and J. L. Manson, Phys. Rev. B **84**, 184402 (2011).
[46] P. A. Goddard, J. L. Manson, J. Singleton, I. Franke, T. Lancaster, A. J. Steele, S. J. Blundell, C. Baines, F. L. Pratt, R. D. McDonald, O. E. Ayala-Valenzuela, J. F. Corbey, H. I. Southerland, P. Sengupta, and J. A. Schlueter, Phys. Rev. Lett. **108**, 077208 (2012).
[47] P. A. Goddard, J. Singleton, I. Franke, J. S. Möller, T. Lancaster, A. J. Steele, C. V. Topping, S. J. Blundell, F. L. Pratt, C. Baines, J. Bendix, R. D. McDonald, J. Brambleby, M. R. Lees, S. H. Lapidus, P. W. Stephens, B. W. Twamley, M. M. Conner, K. Funk, J. F. Corbey, H. E. Tran, J. A. Schlueter, and J. L. Manson, Phys. Rev. B **93**, 094430 (2016).
[48] V. Selmani, C. P. Landee, M. M. Turnbull, J. L. Wikaira, and F. Xiao, Inorg. Chem. Commun. **13**, 1399 (2010).
[49] See Supplemental Material at http://link.aps.org/supplemental/10.1103/PhysRevB.102.064431 for additional information about the material synthesis, crystal structure, magnetometry, ESR spectroscopy, specific heat, MAS NMR, and DFT calculations, which includes Refs [81–94].
[50] CrysAlisPro, Oxford Diffraction/Agilent Technologies UK Ltd, Yarnton, England.
[51] SCALE3 ABSPACK, version: 1.0.4, gui: 1.03; an oxford diffraction program; Oxford Diffraction Ltd: Abingdon, UK (2005) .
[52] G. M. Sheldrick, Acta Cryst. A **64**, 112 (2008).
[53] G. M. Sheldrick, Acta Cryst. C **71**, 3 (2015).
[54] S. Stoll and A. Schweiger, J. Magn. Reson. **178**, 42 (2006).
[55] S. Zvyagin, J. Krzystek, P. van Loosdrecht, G. Dhalenne, and A. Revcolevschi, Phys. B (Amsterdam, Neth.) **346-347**, 1 (2004).
[56] F. M. Woodward, A. S. Albrecht, C. M. Wynn, C. P. Landee, and M. M. Turnbull, Phys. Rev. B **65**, 144412 (2002).
[57] B. C. Keith, C. P. Landee, T. Valleau, M. M. Turnbull, and N. Harrison, Phys. Rev. B **84**, 104442 (2011).
[58] B. C. Keith, C. P. Landee, T. Valleau, M. M. Turnbull, and N. Harrison, Phys. Rev. B **84**, 229901(E) (2011).
[59] A. Bencini and D. Gatteschi, *EPR of Exchange Coupled Systems* (Dover Publications, Mineola, 2012).
[60] P. M. Richards and M. B. Salamon, Phys. Rev. B **9**, 32 (1974).
[61] M. Dumm, A. Loidl, B. W. Fravel, K. P. Starkey, L. K. Montgomery, and M. Dressel, Phys. Rev. B **61**, 511 (2000).
[62] T. Lancaster, S. J. Blundell, M. L. Brooks, P. J. Baker, F. L. Pratt, J. L. Manson, M. M. Conner, F. Xiao, C. P. Landee, F. A. Chaves, S. Soriano, M. A. Novak, T. P. Papageorgiou, A. D. Bianchi, T. Herrmannsdörfer, J. Wosnitza, and J. A. Schlueter, Phys. Rev. B **75**, 094421 (2007).
[63] A. Sandvik and C. P. Landee (unpublished).
[64] S. J. Blundell, Contemp. Phys. **40**, 175 (1999).
[65] T. Lancaster, S. J. Blundell, P. J. Baker, M. L. Brooks, W. Hayes, F. L. Pratt, J. L. Manson, M. M. Conner, and J. A. Schlueter, Phys. Rev. Lett. **99**, 267601 (2007).
[66] A. Samoson, T. Tuherm, J. Past, A. Reinhold, T. Anupold, and I. Heinmaa, Lect. Notes Phys. **246**, 15 (2005).
[67] A. W. Sandvik, Phys. Rev. Lett. **80**, 5196 (1998).
[68] A. Cuccoli, T. Roscilde, V. Tognetti, R. Vaia, and P. Verrucchi, Phys. Rev. B **67**, 104414 (2003).
[69] S. Chakravarty, B. I. Halperin, and D. R. Nelson, Phys. Rev. B **39**, 2344 (1989).
[70] A. Cuccoli, T. Roscilde, V. Tognetti, R. Vaia, and P. Verrucchi, Eur. Phys. J. B **20**, 55 (2001).
[71] B. J. Suh, F. Borsa, L. L. Miller, M. Corti, D. C. Johnston, and D. R. Torgeson, Phys. Rev. Lett. **75**, 2212 (1995).
[72] D. Vaknin, S. K. Sinha, C. Stassis, L. L. Miller, and D. C. Johnston, Phys. Rev. B **41**, 1926 (1990).
[73] H. Benner and J. P. Boucher, in *Magnetic Properties of Layered Transition Metal Compounds*, edited by L. J. de Jongh (Kluwer, Dordrecht, 1990).

[74] P. Sengupta, A. W. Sandvik, and R. R. P. Singh, Phys. Rev. B **68**, 094423 (2003).
[75] S. Vela, A. Sopena, J. Ribas-Arino, J. J. Novoa, and M. Deumal, Chem. Eur. J. **20**, 7083 (2014).
[76] S. Vela, J. Jornet-Somoza, M. M. Turnbull, R. Feyerherm, J. J. Novoa, and M. Deumal, Inorg. Chem. **52**, 12923 (2013).
[77] M. Matsuura, K. Gilijamse, J. E. W. Sterkenburg, and D. J. Breed, Phys. Lett. A **33**, 363 (1970).
[78] P. Sengupta, C. D. Batista, R. D. McDonald, S. Cox, J. Singleton, L. Huang, T. P. Papageorgiou, O. Ignatchik, T. Herrmannsdörfer, J. L. Manson, J. A. Schlueter, K. A. Funk, and J. Wosnitza, Phys. Rev. B **79**, 060409(R) (2009).
[79] N. A. Fortune, S. T. Hannahs, C. P. Landee, M. M. Turnbull, and F. Xiao, J. Phys.: Conf. Ser. **568**, 042004 (2014).
[80] https://wrap.warwick.ac.uk/139957.
[81] A. D. Becke, Phys. Rev. A **38**, 3098 (1988).
[82] M. J. Frisch *et al.*, *Gaussian 09* (Gaussian, Inc., Wallingford CT, 2009).
[83] M. Deumal, M. J. Bearpark, J. J. Novoa, and M. A. Robb, J. Phys. Chem. A **106**, 1299 (2002).
[84] L. C. M. Gorkom, J. M. Hook, M. B. Logan, J. V. Hanna, and R. E. Wasylishen, Magn. Reson. Chem. **33**, 791 (1995).
[85] E. C. Alyea, J. Malito, and J. H. Nelson, Inorg. Chem. **26**, 4294 (1987).
[86] T. Soda, Y. Kitagawa, T. Onishi, Y. Takano, Y. Shigeta, H. Nagao, Y. Yoshioka, and K. Yamaguchi, Chem. Phys. Lett. **319**, 223 (2000).
[87] M. Alla and E. Lippmaa, Chem. Phys. Lett. **87** (1982).
[88] C. Lee, W. Yang, and R. G. Parr, Phys. Rev. B **37**, 785 (1988).
[89] L. Noodleman, J. Chem. Phys. **74**, 5737 (1981).
[90] E. R. Andrew, M. Firth, A. Jasinski, and P. Randall, Phys. Lett. A **31**, 446 (1970).
[91] J. J. Novoa, M. Deumal, and J. Jornet-Somoza, Chem. Soc. Rev. **40**, 3182 (2011).
[92] E. A. Turov, *Physical Properties of Magnetically Ordered Crystals* (Academic Press, New York, 1965).
[93] A. D. Becke, J. Chem. Phys. **104**, 1040 (1996).
[94] L. Noodleman and E. R. Davidson, Chem. Phys. **109**, 131 (1986).